J Mar Sci Technol (2009) 14:359–372
DOI 10.1007/s00773-009-0053-6

ORIGINAL ARTICLE

Wave energy assessments in the Black Sea

Eugen Rusu

Received: 30 November 2008 / Accepted: 3 March 2009 / Published online: 2 April 2009

Abstract The present work aims to evaluate the wave energy resources in the Black Sea basin. The study is focused on the western part of the sea, which is traditionally considered as being more energetic. In order to give a first perspective of the wave climate, a medium-term wave analysis was carried out using in situ measured data. As a further step, a wave prediction system was implemented for the Black Sea. This was based on the simulating waves near-shore model, which is used for both wave generation and near-shore transformation. This methodology has the advantage that a single model covers the full scale of the modelling process. Various tests were performed considering data measured at three different locations. Special attention was paid to the whitecapping process, which is still widely considered to be the weak link in deep water wave modelling. Comparisons carried out against measured data show that the wave prediction system generally provides reliable results, especially in terms of significant wave heights and mean periods. By increasing the resolution in geographical space, the field distributions of wave energy were analysed for both high and average wave conditions. The analysis and the wave prediction system developed are a prerequisite for further investigations extended in time and with increased resolution in the near-shore direction.

Keywords Renewable energy · Black Sea · Surface waves · Wave power · Spectral models

E. Rusu (✉)
University 'Dunarea de Jos' of Galati,
55 Domneasca Str., 800008 Galaţi, Romania
e-mail: erusu@ugal.ro

1 Introduction

The ocean is a vast repository of energy that can be extracted from its motion, temperature, or chemistry. Ocean energy can be recovered from waves, tides, marine currents, thermal gradients, and differences in salinity. Among all these options, the most challenging may be wave energy extraction.

Wave energy technologies extract energy from the movement of the ocean's waves, which are created by wind interacting with the ocean surface, while tidal energy technologies use the powerful water currents created by the rise and fall of the tides. Although not yet quantified, tidal technologies' overall availability appears to be much less than that of wave energy systems since it is only feasible in areas where the tidal currents are strong enough to run turbines efficiently.

Wave energy is abundant and, while not as predictable as tidal energy, is more predictable than wind or solar energy. Although the amount of energy that can be extracted using wave technologies varies from site to site and from day to day, depending on the location and weather conditions, wave energy can be accurately predicted using numerical models within a window of a few days. Constancy and predictability enable a more straightforward and reliable integration into the electricity utility grid. Wave energy also offers much higher energy densities, allowing devices to extract more power from a smaller volume at consequently lower costs.

Interest in extracting power from waves (as distinctly different from flowing water, such as rivers or tides) began in earnest in the 1970s. Unfortunately, none of the schemes developed at that time was able to achieve a full-scale trial. The field remained largely quiet until the past decade, when the success of the wind power industry spurred

renewed interest in discovering what might work in the sea. Wave-energy extraction is at this moment, in a real sense, where wind power was 15 or 20 years ago, with no clearly superior engineering solutions. However, around the world, various research teams are currently making progress in devising effective and efficient means for tapping wave energy, and it is becoming more and more obvious that wave power will play an important role in the global energy portfolio.

The highest energy ocean waves are concentrated off western coasts in the 40–60° latitude range north and south. Waves are bigger and more powerful along the western edge of the continents because of the prevailing west-to-east winds. The annual average power in the wave fronts varies in these areas between 30 and 70 kW/m, with peaks up to 100 kW/m in the Atlantic southwest of Ireland, in the Southern Ocean, and close to Cape Horn. Chile, Australia, New Zealand, Ireland, the UK, Portugal, and Norway have substantial wave power potential due to features they all share: a location in a relatively high latitude and a long stretch of ocean immediately to the west.

Although not included among areas richest in wave energy resources, the Black Sea basin may offer potential for development, since very strong wind patterns induce an energetic regime often comparable, in terms of wave heights, to oceanic sites. In this context, the objective of the present work is to explore the wave energy resources in the Black Sea. The study will be focused mainly on the western part, which is the most energetic region of the entire sea.

2 Analysis of the wave climate in the western Black Sea

Some features of the wave climate in the western section of the Black Sea will be presented in this section. Three different data sources were considered.

2.1 Analysis of near-shore data

The first analysis concerns near-shore data measured during the period 1971–1994 in the coastal environment close to Constanta harbour as presented by the Marine Research Institute Grigore Antipa [1]. The principal wind directions computed for each month, and given as percentage of the time, are presented in Table 1, while the monthly average wind velocities are presented in Table 2.

From the data in the above tables, it can be observed that the wind coming from the northern sector (NW, N, and NE), is dominant, representing about 40.3% of the annual

Table 1 Wind frequencies (percentage) corresponding to the principal directions computed for each month, according to INCDM [1]

	I	II	III	IV	V	VI	VII	VIII	IX	X	XI	XII	Yearly
N	20.7	22.2	18.4	11.0	9.5	9.1	13.2	13.3	14.5	21.6	17.9	17.7	15.8
NE	10.5	16.8	20.9	13.1	11.9	8.8	10.4	13.7	12.5	13.9	9.7	8.0	12.5
E	3.0	4.3	7.4	9.0	10.8	7.7	8.1	9.7	10.7	6.7	5.6	2.4	7.1
SE	3.3	6.4	11.9	16.9	19.4	16.9	13.3	11.5	13.0	11.3	6.4	3.7	11.1
S	9.6	10.3	13.8	20.5	19.4	19.3	15.6	13.0	14.7	13.1	11.3	9.3	14.1
SW	11.3	7.8	7.6	7.1	7.4	8.9	7.6	7.0	7.7	9.2	10.3	11.4	8.6
W	28.0	18.8	11.7	13.3	13.2	18.0	17.4	15.9	18.1	14.2	24.4	31.0	18.7
NW	13.6	13.4	8.4	9.3	8.3	11.3	14.4	14.9	9.7	9.9	14.4	16.4	12.0

Table 2 Wind velocities (m/s) corresponding to the principal directions computed for each month, according to INCDM [1]

	I	II	III	IV	V	VI	VII	VIII	IX	X	XI	XII	Yearly
N	8.5	8.4	7.5	6.4	5.7	5.6	5.7	6.2	6.7	7.9	7.8	8.5	7.4
NE	8.7	7.7	6.7	5.8	5.6	5.1	5.1	5.5	6.2	7.3	7.9	8.7	6.7
E	6.3	4.7	4.3	3.9	3.9	3.6	3.7	3.7	3.9	5.1	6.5	6.7	4.3
SE	4.7	4.0	3.9	4.2	3.9	4.2	3.7	3.6	4.1	4.1	4.3	4.5	4.0
S	4.6	4.4	4.4	4.4	4.0	4.1	3.8	3.8	3.8	4.1	4.4	4.7	4.2
SW	4.0	4.1	3.8	4.2	3.8	3.2	2.7	2.8	3.1	3.2	3.6	4.0	3.6
W	4.4	4.3	4.6	4.5	4.0	4.0	3.5	3.2	3.7	3.7	4.0	4.3	4.0
NW	4.7	4.9	4.8	4.8	4.3	4.5	4.5	4.4	4.8	4.9	4.8	4.8	4.7
V_{med}	5.78	5.85	5.40	4.77	4.33	4.25	4.13	4.24	4.59	5.37	5.34	5.54	4.97

V_{med} average wind velocity

total, while the wind coming from the southern sector represents 33.8%. The highest annual velocities were recorded for wind coming from the northern sector. The average wind velocity and also the periods of calm have a quite pronounced cyclic evolution.

The wave fields in the study area are characterized by significant variations during the year. The annual average evolution of periods of calm (i.e., significant wave heights smaller than 0.2 m) as well as of the alternating occurrence of wind seas and swell are illustrated in Fig. 1a. From this figure it is observed that the duration of the periods of calm is maximum in May (about 66.5% of the total time) and minimum in October (42.1%). Wind seas occur 20.3% of the time in May and 39.4% of the time in October and swells occur 13.1% in June and 20.6% in November; the ratio between wind seas and swell being about 1.2 in November and 2.2 in October.

The dominant wind from the northern sector is reflected by the fact that most of the wind waves were observed to propagate from the northwest (41.2%, for NE, N, and E), whereas, because of wave refraction, the dominant swell direction is from the east (31.1%), together with the adjacent directions. The highest average values of the wave parameters are encountered in directions approximately normal to the coast (E); i.e., 1.2 m significant wave height, 5.2 s mean period, and 34 m wavelength as illustrated in Fig. 1b.

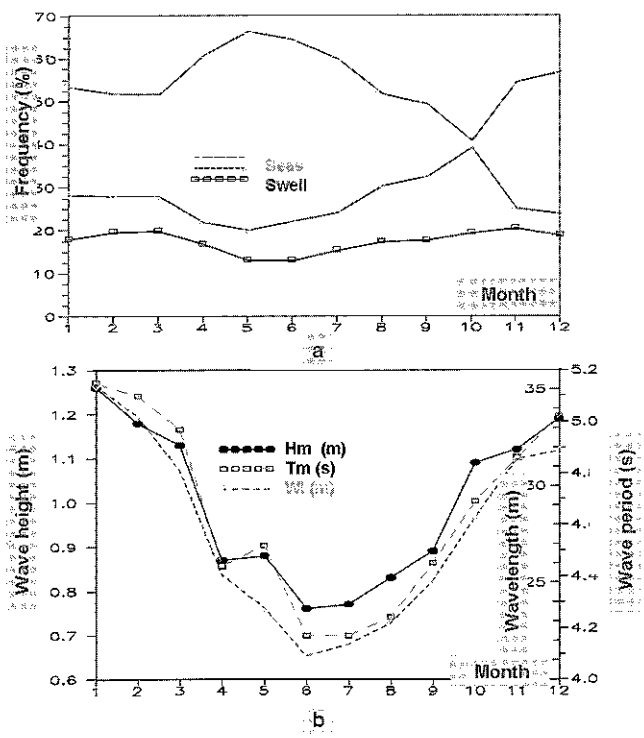

Fig. 1 Wave climate analysis close to Constanta harbour for the period 1971–1994 (according to [1]). **a** Average annual evolution (in percentage) of the periods of calm, wind seas, and swell. **b** Monthly averaged values of the main wave parameters: mean wave height (*Hm*), mean period (*Tm*) and wavelength (*Wl*)

2.2 Analysis of offshore data

This analysis is based on data measured at the Gloria drilling platform, which operates in the western sector of the Black Sea (44°31′N, 29°34′E) at a location where the water depth is about 50 m. The measurements were performed daily during a 3-year period between 2002 and 2004 at 6-h intervals; the percentage of valid data was about 94%.

Much of the annual wave energy occurs during wintertime, so results will be reported for the whole year and for wintertime only. Here, wintertime is considered to be the 6-month period extending from October through March.

The results from the measurements are presented in Fig. 2 and they include the classes of significant wave height (Fig. 2a, b), mean periods (Fig. 2c, d), and also the wave direction distributions (Fig. 2e, f), all corresponding both to the whole year (left side) and wintertime (right side). The monthly maximums and average values of the wave heights and wave periods are shown in Fig. 2g, h, respectively.

From the analysis of the results presented in Fig. 2, the following features of the wave climate in the area of analysis can be identified:

- The month of December has the highest probability of occurrence of waves with heights greater than 7 m (6.88%), the possibility of this occurrence begins in September and lasts through April. An identical evolution is seen for the wave heights in the classes 5–6 and 6–7 m (for this last case, the highest frequency of occurrence is in February and represents 5.45% of the total). For the class of 4–5 m, approximately equal peaks were encountered in October, December, and February.
- The frequency of occurrence of wave heights greater than 4 m is greatest in February (20.44%), whereas no such waves occur in June. Waves of the classes 2–3 and 3–4 m are present throughout the year with a frequency fairly equilibrated between summertime (59.94%) and wintertime (60.31%).
- Waves with heights between 1 and 2 m occur approximately equally throughout the year, with a minimum in March and a maximum in July. The results are not the same for waves with heights smaller than 1 m; these have a frequency of occurrence in summertime almost double that of wintertime.
- Regarding wave periods, values greater than 9 s were encountered only in January, and periods greater than 7 s are characteristic of wintertime only. The other two classes of wave periods are evenly distributed over the

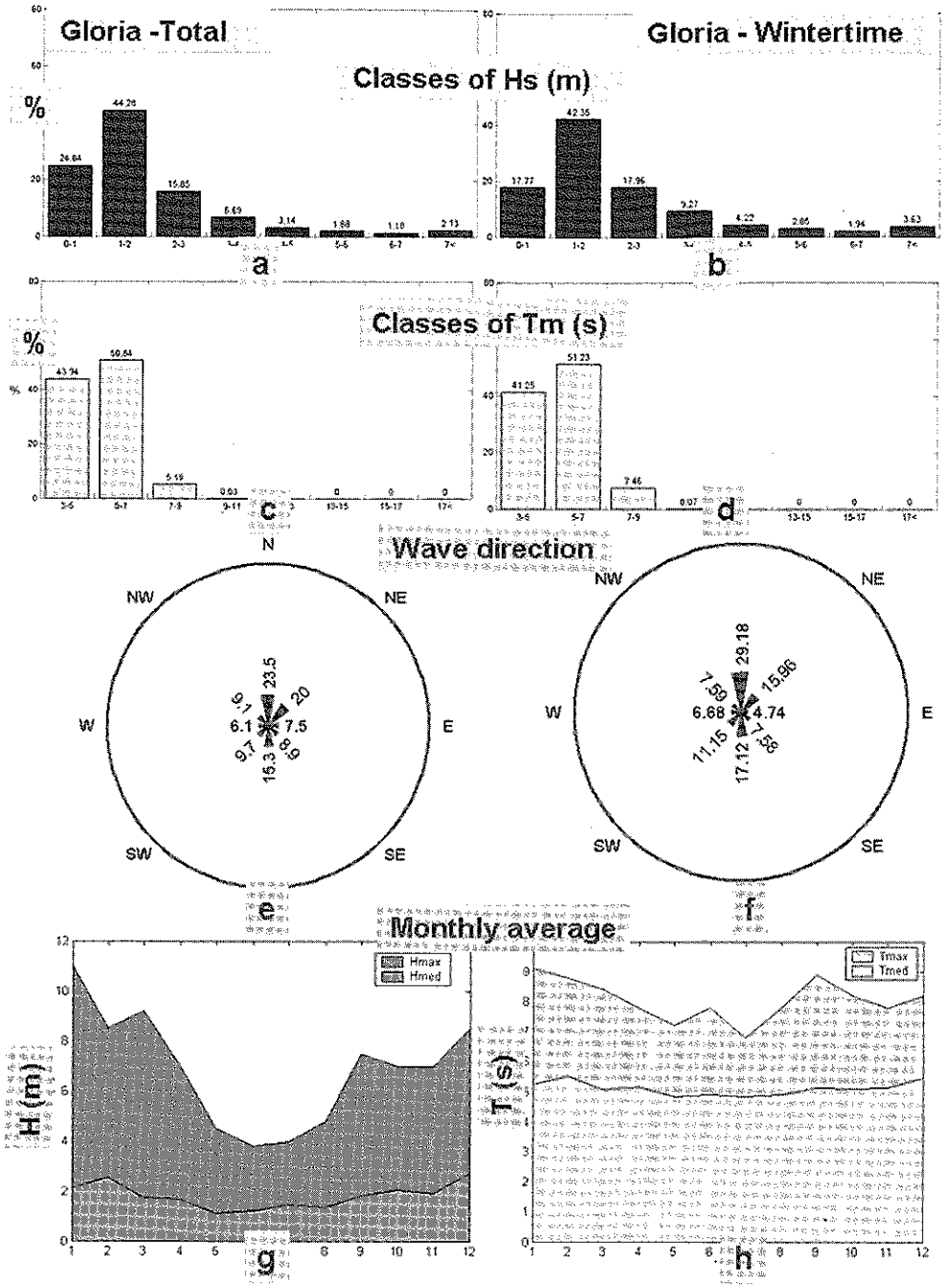

Fig. 2 Analysis of the wave data measured at Gloria drilling platform in the period 2002–2004. **a** Classes of significant wave height (*Hs*) for total time interval; **b** classes of *Hs* for wintertime; **c** classes of *Tm* for total time interval; **d** classes of *Tm* for wintertime; **e** mean wave direction distribution for total time interval; **f** mean wave direction distribution for wintertime; **g** monthly averaged values for the medium and maximum wave height; **h** monthly averaged values for the medium and maximum wave period

year with the observation that, in December, a significant enhancement occurs of periods from the class 5–7 s (60.73%), while the periods from the class 3–5 s represent only a 32.79%.

- The dominant wave direction is from the northern sector (NW, N, NE) both for winter (52.73%) and summer (52.25%). For the southern sector (SE, S, SW), the percentages are 35.85% for winter and 31.7% for summer.

Analysis of the wave heights indicates that the highest average values are characteristic of waves coming from the northern sector, with a maximum of 5.36 m for the north direction. For wave periods, the highest average value corresponds to waves coming from the northeast and is 5.63 s. Table 3 presents the average significant wave heights corresponding to the principal directions computed for each month.

2.3 Storm analysis

Coman [2] presented an analysis of the storms that affected the Romanian coastal environment during the period 1980–

Table 3 Average significant wave heights (m) corresponding to the principal directions computed for each month (data recorded at the Gloria drilling platform in the period 2002–2004)

	N	NE	E	SE	S	SW	W	NW
I	2.47	2.24	1.19	1.94	1.95	1.68	1.72	**2.61**
II	**3.42**	2.67	0.55	2.26	2.33	0.98	1.39	3.07
III	**2.86**	1.61	0.68	1.23	1.23	1.4	1	1.52
IV	1.25	**2.23**	0.92	1.67	1.72	1.33	1.41	1.8
V	**1.81**	1.07	0.92	0.7	1.31	0.61	0.85	1.07
VI	1.33	1.06	**1.52**	1.16	1.43	0.94	0.85	1.28
VII	1.29	1.84	1.03	**1.95**	1.26	1.22	1.54	1.16
VIII	1.51	1.23	0.88	1.67	1.54	**1.73**	1.13	1.48
IX	1.66	**2.95**	1.96	0.84	1.9	0.88	1.93	1.33
X	2.09	**2.54**	2.09	1.37	2.16	1.6	1.92	2.42
XI	2.78	**3.03**	1.7	1.31	1.3	1.55	1.39	1.98
XII	**3.3**	3.10	2.16	1.63	2.52	1.71	1.17	1.63

The maximum value for each month is in *bold*

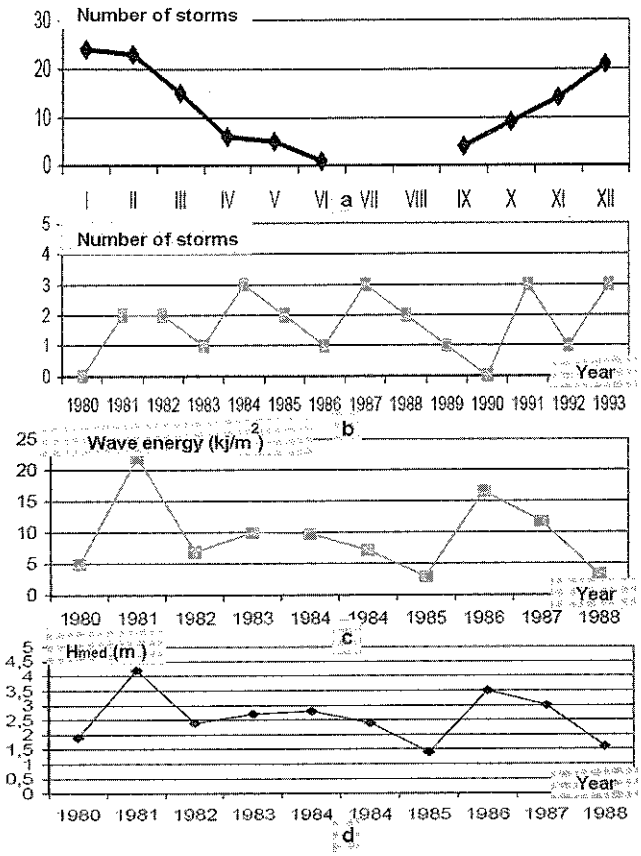

Fig. 3 Storm analysis. **a** Monthly distribution of the total number of storms (for the period 1980–1993); **b** annual distribution of the storms with duration greater than 72 h (for the period 1980–1993); **c** wave energy corresponding to the strongest storms (for the period 1980–1988); **d** average wave height corresponding to the strongest storms (for the period 1980–1988)

1993. Some conclusions of this study are illustrated in Fig. 3 and will be briefly discussed below.

The average storm duration was about 30 h and the maximum storm duration was about 130 h. Most of the storms were generated from winds coming from the northern sector. Figure 3a illustrates the monthly distribution of the total number of storms and Fig. 3b the annual distribution of the storms with duration greater than 72 h (for the entire period analyzed 1980–1993).

The calculated average wave energies and wave heights for storms lasting longer than 3 days are presented in Fig. 3c, d. These figures show that, for the storms of January 1981 and February 1986, the average values were the greatest, and they also illustrate the direct relationship that exists between the wave energy and the significant wave height.

Hence, the above analysis may provide an initial picture concerning the energetic climate in the western side of the Black Sea basin. Some general observations would be that the most energetic months are February and December (as presented in Table 3), while the most energetic wave directions in the offshore area are north to northeast. Table 3 also illustrates, as a first approach, the monthly fluctuation of wave energy in the targeted area, which is important for planning and designing wave energy utilization systems.

3 Description of the wave prediction system

The most accurate estimation of wave fields is provided nowadays by spectral phase averaging models. Among them, WAM [3] and simulating waves near-shore (SWAN) [4] are considered state-of-the-art models for wave generation and coastal transformation, respectively. The basic scientific philosophy of these two models is similar, as they are both third-generation wave models based on solving the energy balance equation in spectral form and they use the same formulations for the source terms, although SWAN uses adapted code for the discrete interaction approximation technique in the parameterization of the quadruplet interactions. SWAN also employs some additional formulations, primarily for shallow water, referring to processes such as triad non-linear interactions, bottom friction, and depth-induced wave breaking.

In the past few years, the capabilities of the model have been substantially extended both in offshore and near-shore directions. As regards the offshore extension, the main improvements are: the high-order S&L propagation scheme of Stelling and Leendertse [5], which is almost free of the numerical diffusion that is associated with large-scale propagations in the non-stationary mode, and the parameterization to counteract the "garden sprinkler

effect" [6], which may show up due to small numerical diffusion associated with a reduced resolution in the spectral space. To extend the performance of the model in the near-shore region, the most recent major improvement concerns designing a phase decoupled approach to account for the diffraction effect [7]. Together with the wave-induced set up, diffraction is adequate for local scale simulations and both these two processes are associated mainly with a Cartesian coordinate system.

Hence, although probably not as computationally efficient as Wave Watch 3 (WW3) or WAM at oceanic scales, at sub-oceanic scales, SWAN currently seems to be the most appropriate wave model. The main reason is its greater flexibility, since it includes various alternatives for modelling and tuning physical processes, either in shallow or deep water. By calibrating the model, an appropriate combination of physical processes and parameters can be identified for a particular site. This leads to better-quality predictions of the main wave parameters. Another advantage is that a single model can be employed for the full range of wave modelling processes, and the focusing of the wave prediction system in the near-shore direction is thus straightforward.

Like most phase averaging models, SWAN solves the spectral energy balance equation that describes the evolution of the wave spectrum in time, geographical, and spectral spaces [8]. The spectrum that is considered is the action density spectrum (N), rather than the energy density spectrum (E), since in the presence of currents, the action density is conserved, whereas energy density is not. The action density is equal to the energy density divided by the relative frequency (σ). Hence, the spectral action balance equation is given by:

$$\frac{\partial N}{\partial t} + \nabla\left[(\vec{c}_g + \vec{U})N\right] + \frac{\partial}{\partial\sigma}c_\sigma N + \frac{\partial}{\partial\theta}c_\theta N = \frac{S}{\sigma}, \tag{1}$$

where θ is the wave direction and $\vec{U}$ is the velocity of the ambient current, which is considered uniform with respect to the vertical coordinate. The propagation velocities of the wave energy are the group velocity $\vec{c}_g$ in physical space ($\vec{c}_g = \partial\sigma/\partial\vec{k}$) and $c_\sigma = \dot{\sigma}$ and $c_\theta = \dot{\theta}$ in spectral space. $\vec{k}$ is the wave number vector related to the relative frequency through the dispersion relationship. For large-scale applications, this equation is related to the spherical coordinates defined by longitude λ and latitude ϕ:

$$\frac{\partial N}{\partial t} + \frac{\partial}{\partial\lambda}c_\lambda N + \frac{1}{\cos\phi}\frac{\partial}{\partial\phi}c_\phi N\cos\phi + \frac{\partial}{\partial\sigma}c_\sigma N + \frac{\partial}{\partial\theta}c_\theta N = \frac{S}{\sigma}. \tag{2}$$

On the right hand side of the action balance equation is the source (S) expressed in terms of energy density. In deep water, the source comprises three primary components: the atmospheric input (S_{in}), whitecapping dissipation (S_{dis}), and nonlinear quadruplet interactions (S_{nl}). In shallow water, additional phenomena such as bottom friction, depth-induced wave breaking, and triad non-linear wave–wave interactions induced by the finite depth effects (S_{fd}) may play an important role. Hence the total source becomes:

$$S_{total} = S_{in} + S_{dis} + S_{nl} + S_{fd}. \tag{3}$$

Studies of shallow water wave processes and quantification of their impacts in the high-resolution areas are topics beyond the scope of the present work, which is focused mainly on modelling offshore wave conditions. In this regard, options available in SWAN for deep water wave modelling will be discussed in the next section, as well as the parameterization used to optimize the model to the specific conditions of the Black Sea basin.

4 Validation tests in the time domain

The computational domain considered for the present SWAN implementation is illustrated in Fig. 4. The system origin corresponds to the lower left corner point and has the coordinates (27.5°, 41.0°). The x direction (longitude) extends 14° and the y direction (latitude) extends 6°,

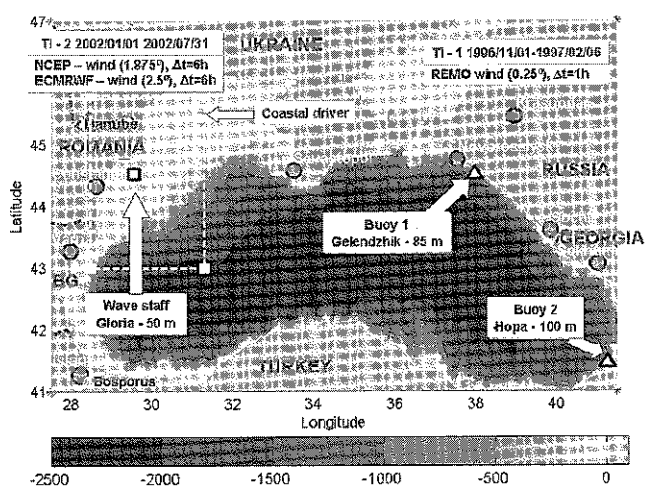

Fig. 4 Bathymetric map of the Black Sea basin corresponding to the computational domain and the locations of the three data sources available. The two time intervals considered are also indicated in the figure: *TI-1* (November 1, 1996–February 6, 1997), when the high-resolution regional model (*REMO*) wind field was available and comparisons against the two buoys were performed, and *TI-2* (January 1, 2002–July 31, 2002), when National Centers for Environmental Prediction (*NCEP*) and European Centre for Medium Range Weather Forecasts (*ECMRWF*) wind fields were used and comparisons against the wave staff were performed. For the second time interval, a medium-resolution area, denoted as coastal driver, was connected to the main computational domain

covering both the Black Sea and the Sea of Azov. In geographical space the computational grid was chosen to coincide with the bathymetric grid and has 176 points in the x direction and 76 points in the y direction. The points are equally spaced with $\Delta x = \Delta y = 0.08°$. In spectral space, 24 directions and 30 frequencies were assumed. The frequency range considered fell between 0.06 and 1.2 Hz.

To assess the spatial distribution of wave energy, the objective at this level was to implement and validate a wave prediction system for the Black Sea basin. This system is entirely based on the SWAN model, which is used for both wave generation and near-shore transformation.

Three check points were considered for model calibration and for performing validation tests. First, data coming from two directional buoys operating in deep water close to the east coast were considered. As a second step, the reliability of the SWAN model results was tested on the west coast using two different wind fields. Results were compared with measurements provided by a wave staff located at the Gloria drilling platform that is operating in the area.

These studies were focused on how well the formulations available in the SWAN model were able to account for whitecapping dissipation. This is because whitecapping still is widely considered to be the weak link in deep water wave modelling and it is closely related to the process of wave generation.

Four different formulations are available to account for the processes of wave generation by wind and whitecapping dissipation. These are: (a) Komen's parameterization [9], which describes the transfer of wind energy to waves coupled with the pulse-based model of Hasselmann [10] for whitecapping dissipation and adapted by the Wave Model Development and Implementation (WAMDI) group (1988) to apply to a finite water depth; (b) Janssen's model for atmospheric input [11] coupled with the same pulse-based model of Hasselmann [10] for whitecapping; (c) Komen's model coupled with the cumulative steepness method (CSM) [12] for whitecapping; and (d) Yan's model for atmospheric input [13] coupled with the saturation-based model of Alves and Banner [14] for whitecapping (denoted in this work as A&B).

The first parameterization (Komen–Hasselmann) corresponds also to WAM cycle 3, while the second parameterization (Janssen–Hasselmann) corresponds to WAM cycle 4. CSM is an alternative formulation for whitecapping and, in this method, dissipation due to whitecapping depends on the steepness of the wave spectrum at and below a particular frequency. A second alternative for the whitecapping expression uses the formulation of Alves and Banner [14]. This expression is based on experimental findings that whitecapping dissipation appears to be related to the nonlinear hydrodynamics within wave groups. This yields a dissipation term that primarily depends on quantities that are localized in the frequency spectrum, as opposed to ones that are distributed over the spectrum, as in the expression of Komen et al. [9]. This whitecapping expression is used together with a wind input term that is based on the work of Yan [13].

As indicated in Fig. 4, two time intervals were considered for model system calibration and for performing the validation tests. The first phase corresponded to the time interval between November 1, 1996 and February 6, 1997, and is denoted TI-1. For this interval, model results were compared with data from the two buoys operating on the east coast of the sea, i.e., Gelendzhik (37.98°E, 44.51°N), denoted as Buoy 1, and Hopa (41.38°E, 41.42°N), denoted as Buoy 2. They are both located in deep water at depths of 85 and 100 m, respectively.

The wind field for this period was provided by the Hindcast of Dynamic Processes of the Ocean and Coastal Areas of Europe (HIPOCAS) project, developed under the framework of the European Program Energy, Environment and Sustainable Development [15, 16], which undertook the re-analysis of wind conditions for the 44-year period between 1958 and 2001. During this first phase, for wave simulations for the time interval TI-1, the global National Centers for Environmental Prediction (NCEP) re-analysis wind was used as a driver for the regional atmosphere model (REMO). The spatial resolution of the wind model output was 0.25° and the time step was 1 h.

4.1 SWAN comparison with Buoy 1 data (calibration process)

Simulations were performed employing most of the possibilities for tuning the SWAN model to account for deep water wave processes. As mentioned previously, four options are currently available in the SWAN model to account for whitecapping dissipation and wave generation by wind. Two use the pulse-based model of Hasselmann for whitecapping coupled with the wind input formulations of Komen or Janssen. The other two options in the current SWAN version (40.72) are CSM and the saturation-based model (denoted in the present work as A&B). CSM uses the wind input formulation of Komen while A&B uses the wind input formulation of Yan [13]. The corresponding results are presented in Table 4 for the time interval TI-1.

Analysis of the statistical data shows that, for most of the parameters studied (i.e., significant wave height, mean period, peak period, and mean wave direction), the best agreement with Buoy 1 data was found using the A&B formulation, followed closely by Komen's formulation. The results also indicate that the A&B formulation not only

Table 4 Gelendzhik directional buoy (Buoy 1) wave statistics ($n = 684$) for the period TI-1 (November 1, 1996–February 6, 1997) and results from all four formulations available for modelling whitecapping dissipation

	Measured	Modelled	Bias	RMSE	SI	r
Komen's parameterization						
Hs (m)	1.004	1.014	−0.010	0.365	0.364	0.886
Tm (s)	3.975	3.411	0.564	0.893	0.225	0.797
Tp (s)	5.609	5.164	0.444	1.486	0.265	0.640
Dir (°)	214.95	204.28	10.664	53.216	0.248	0.449
Janssen's model						
Hs (m)	1.004	1.043	−0.039	0.469	0.467	0.808
Tm (s)	3.975	4.032	−0.058	0.855	0.215	0.701
Tp (s)	5.609	5.566	0.043	1.588	0.283	0.525
Dir (°)	214.95	224.52	−9.568	68.604	0.319	0.318
CSM						
Hs (m)	1.004	1.107	−0.104	0.429	0.428	0.848
Tm (s)	3.975	3.321	0.653	0.991	0.249	0.745
Tp (s)	5.609	5.873	−0.264	1.554	0.277	0.576
Dir (°)	214.95	221.92	−6.971	67.110	0.312	0.395
A&B						
Hs (m)	1.004	1.004	0.000	0.361	0.360	0.888
Tm (s)	3.975	3.790	0.185	0.826	0.208	0.767
Tp (s)	5.609	5.563	0.045	1.485	0.265	0.618
Dir (°)	214.95	208.95	6.000	53.540	0.269	0.432

RMSE root mean square error, *SI* scatter index, *CSM* cumulative steepness method, *A&B* saturation-based model of Alves and Banner, *Hs* significant wave height, *Tm* mean period, *Tp* peak period, *Dir* mean wave direction

yields the best predictions, but also requires the smallest variation of the tuneable coefficients.

Results were also compared with those generated by the WAM model using exactly the same wind data field [17] for the same time interval, TI-1. Examining the values of the statistical parameters, it is apparent that the SWAN results are considerably better than the WAM results for any of the whitecapping parameterization methods considered. This probably is due to the better flexibility in tuning the parameters in the SWAN model. Thus, the biases obtained for the WAM model for the same time interval were 0.27 for Hs, 0.43 for Tp, and 33.1 for Dir. Referring to the RMSE, the values obtained were 0.53 for Hs, 1.74 for Tp, and 92.7 for Dir, which means considerably higher RMSE values at least with regard to the significant wave height and the mean direction. The scatter indices obtained were 0.68 for Hs, 0.34 for Tp, and 0.46 for Dir, which also mean that the results of the SWAN model are better. Finally, the computed correlation coefficients for the WAM data were 0.73 for Hs, 0.55 for Tp, and 0.36 for Dir. This indicates that the SWAN results agreed better with the measured data than the WAM results.

Table 5 Hopa directional buoy (Buoy 2) wave statistics ($n = 465$) and modelled values for the period TI-1

	Measured	Modelled	Bias	RMSE	SI	r
Komen's parameterization						
Hs (m)	0.565	0.646	−0.081	0.325	0.576	0.781
Tm (s)	4.142	3.722	0.420	0.998	0.241	0.699
Dir (°)	253.48	301.43	−47.950	107.49	0.424	0.133
A&B						
Hs (m)	0.565	0.552	0.013	0.297	0.526	0.814
Tm (s)	4.142	4.309	−0.166	1.110	0.268	0.585
Dir (°)	253.48	294.29	−40.81	102.72	0.405	0.241

The parameterization containing Komen's formulation for wind growing combined with the pulse-based model of Haselmann for whitecapping dissipation was tested in parallel with the new parameterization combining Yan's formulation for wind growing with the saturation-based model of Alves and Banner for whitecapping

4.2 SWAN compared with Buoy 2 (first validation test)

The performance of the model was also assessed in the southern portion of the east coast for the same time interval (TI-1). The Hopa directional buoy was operating in that area and its location is shown in Fig. 4. This time, only the Komen and A&B whitecapping formulations were evaluated, since they were found to be more effective in the previous case. The corresponding results are presented in Table 5.

As can be seen from the table, significant wave height results provided by the A&B formulation are still better than those obtained with the Komen–Hasselmann approach; however, the Komen formulation gives slightly better results for the mean period. Although the models do not provide very accurate predictions of the mean directions, the A&B formulation performs slightly better. When compared with the results for Buoy 1 (as presented in Table 4), it can be seen that significant wave heights are better estimated at Buoy 2 in terms of RMSE and at Buoy 1 in terms of scatter indices. The mean periods and mean directions are better estimated at Buoy 1.

4.3 Validation on the west coast (second validation test)

As a second validation test, model simulations were performed for the time interval between January 1, 2002 and July 31, 2002 (denoted TI-2). Two different wind fields were used: NCEP (1.875° spatial resolution) and European Centre for Medium Range Weather Forecasts (ECMRWF) (2.5° spatial resolution); the temporal resolution was 6 h for both fields. Data measured in situ by a wave staff placed at the Gloria drilling platform were used as a reference. The drilling unit operates in the western coastal environment of the Black Sea in about 50 m of water (Fig. 4), and both wind and

wave measurements were available for the period considered. Since the wave staff was located at an intermediate water depth, a second area was connected to the main computational domain in order better to account for the coastal wave transformation, as illustrated in Fig. 4.

A comparison of the measured wind velocities with the predictions of the two different model approaches was first carried out. Wind velocities recorded at 28 m height were adjusted to 10 m using the simple relationship from Hsu et al. [18]

$$u_2 = u_1(z_2/z_1)^P, \tag{4}$$

where u_2 denotes the wind speed at the reference height z_2 (28 m), and u_1 represents the wind speed at height z_1 (10 m). The exponent, P, was set to 0.11, which is considered typical for sea conditions. Comparisons indicate that the wind model predictions were generally reliable. The NCEP wind fields appear to be more accurate; however, the atmospheric models seem to systematically underpredict the wind velocities (positive biases).

Using the Komen and A&B formulations, SWAN simulations were performed considering the NCEP and ECMRWF wind fields. As expected, the NCEP field provided better results than ECMRWF in terms of the wave parameters. Direct comparisons of measured significant wave heights and mean periods and model results using the NCEP wind field are illustrated in Fig. 5. The corresponding statistical results are presented in Table 6 and scatter plots for the significant wave heights and mean periods are given in Fig. 6. The results are again slightly better when the A&B formulation is used. Nevertheless, the results are, in general, less accurate than for the case discussed in the previous section when the wind resolution was better both in space and time. Although the wave measurements at the staff were non-directional, direction was indicated based on visual observations by the human operator (S, SW, W, etc.). The model predictions agreed with 88.4% of these observations.

At high energetic conditions, significant wave height peaks seem to be systematically underestimated by the model when the A&B formulation is used; the Komen formulation appears to be more effective in this high energetic range. To account for this and to improve the performance of the model, the A&B formulation could be employed for low and moderate energetic conditions, and the Komen formulation could be applied for high energetic conditions.

5 Energetic patterns in the Black Sea

In the SWAN model, the energy transport components (expressed in watts/metre, i.e., energy transport per unit length of wave front), are computed with the relationships:

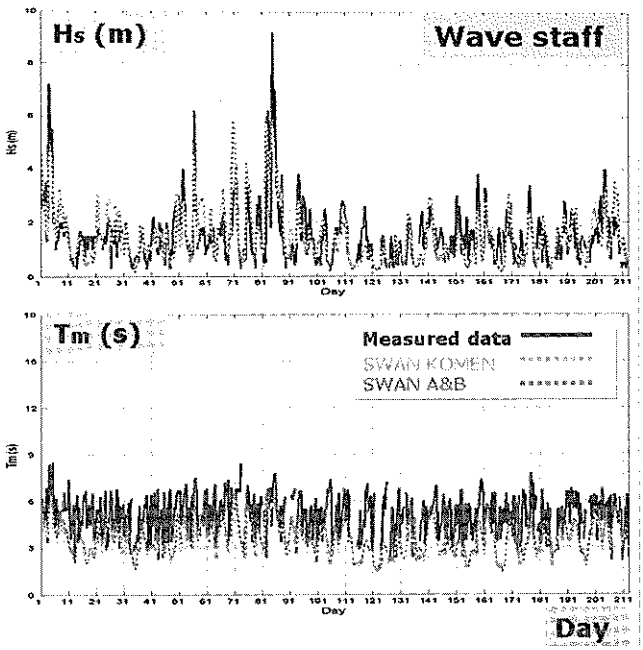

Fig. 5 Direct comparisons on the west coast of the results of the simulating waves near-shore model (*SWAN*) forced with the NCEP wind field, against wave staff measurements (*Hs* and *Tm*). Days relate to period TI-2. The results provided by the Komen–Hasselmann (*SWAN KOMEN*) and Yan-A&B (*SWAN A&B*) parameterizations to model wave generation and whitecapping dissipations are illustrated in parallel

Table 6 Gloria drilling platform (wave staff) wave statistics and modelled values for period TI-2 (January 1, 2002–July 31, 2002) ($n = 781$)

	Measured	Modelled	Bias	RMSE	SI	r
Komen's parameterization						
Hs (m)	1.535	1.551	−0.016	0.762	0.496	0.709
Tm (s)	5.08	3.339	1.741	2.191	0.431	0.221
A&B						
Hs (m)	1.535	1.520	0.015	0.758	0.494	0.724
Tm (s)	5.08	3.744	1.336	1.941	0.382	0.234

$$P_x = \rho g \iint c_x E(\sigma,\theta)\mathrm{d}\sigma\,\mathrm{d}\theta$$
$$P_y = \rho g \iint c_y E(\sigma,\theta)\mathrm{d}\sigma\,\mathrm{d}\theta, \tag{5}$$

where x, y are the problem coordinate system (for the spherical coordinates, the x axis corresponds to longitude and the y axis to latitude), and c_x and c_y are the propagation velocities of wave energy in geographical space defined as:

$$\frac{\mathrm{d}\vec{x}}{\mathrm{d}t} = (c_x, c_y) = \vec{c}_g + \vec{U}. \tag{6}$$

Hence the absolute value of the energy transport (denoted also as wave power) will be:

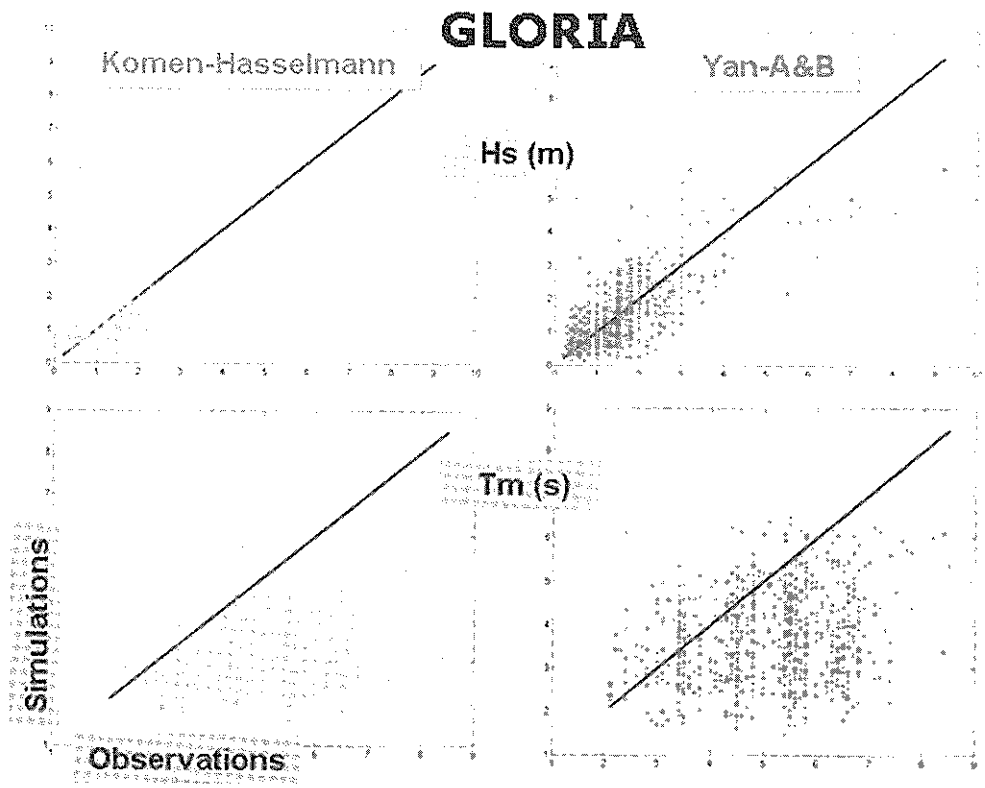

Fig. 6 Scatter plots for the main non-directional wave parameters (Hs and Tm), SWAN results against wave staff measurements at Gloria drilling platform for time interval TI-2. The *left side* corresponds to Komen–Hasselmann parameterization while the *right side* to Yan-A&B

$$P = \sqrt{P_x^2 + P_y^2}. \tag{7}$$

Four case studies of wave energy distributions are presented below. Two of them correspond to the entire Black Sea basin, while the other two correspond to a medium-resolution domain covering the Romanian coastal environment on the western side of the Black Sea. For each case study, significant wave height scalar fields are presented together with the wind and wave vectors, along with the normalized wave power and the energy transport vectors.

The non-dimensional normalized wave power is expressed as:

$$P_n = \frac{P}{P_{t\max}}. \tag{8}$$

In the present work $P_{t\max}$ was defined separately for each individual case study and approximates the maximum wave power corresponding to the computational domain.

5.1 Case study 1: midday on January 12, 1997

This case study provides an average energy distribution for the entire Black Sea basin and is illustrated in Fig. 7. Figure 7a presents the significant wave height scalar field in the background and the wave vectors (black arrows) and wind vectors (white arrows) in the foreground. Figure 7b shows the normalized wave power in the background and the energy transport vectors (in kilowatt/metre of wave front) in the foreground. The locations of the maximum values of significant wave height, wind velocity, and wave power for this computational domain are marked with circles. For this case study the value of $P_{t\max}$ was set at 20 kW/m.

Some observations arise from the analysis of the above results. Although there is an obvious relationship between significant wave height and wave power, the energetic peak in a computational domain is not necessarily located at the same point as (or even close to) the maximum significant wave height. This is very well illustrated by the results presented in Fig. 7a, b, where the overall energetic peak (20 kW/m) is located on the southern side of the sea while the maximum significant wave height (3.1 m) is on the western side.

5.2 Case study 2: January 21, 1997, at 1800 hours

This second case study presents some storm conditions in the Black Sea and is illustrated in Fig. 8. It should be noted that this is not an extreme event, but a regular storm (moreover it is a typical storm when the western part of the Black Sea is more energetic due to the dominant wind patterns).

Figure 8a presents the significant wave height scalar field in the background and the wave and wind vectors in

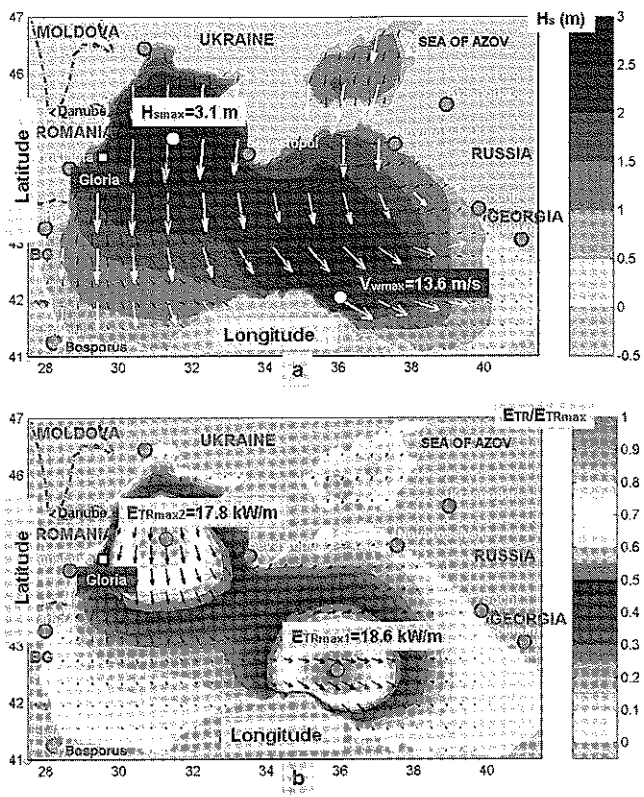

Fig. 7 Case study 1—midday on January 12, 1997—average energetic situation, representation of the entire Black Sea basin. **a** The *background shades* of *blue* indicate the significant wave height scalar field and in the *foreground* are wave vectors (*black arrows*) and wind vectors (*white arrows*). **b** The *background* shows normalized wave power (E_{TR}/E_{TRmax}) and the *foreground* shows energy transport vectors (in kilowatts per metre of wave front). The locations in the computational domain of the maximum values for the significant wave height, wind velocity, and wave power are marked with *circles*

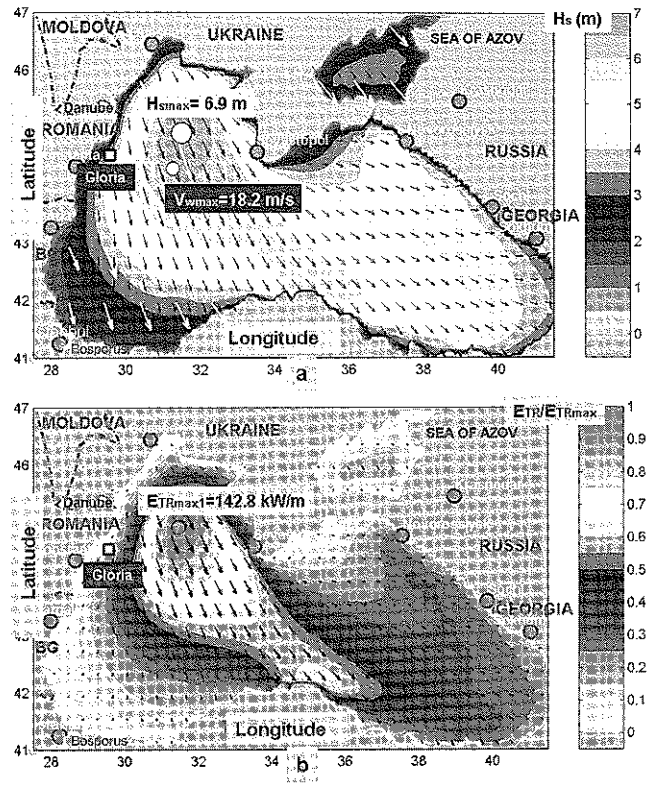

Fig. 8 Case study 2—January 21, 1997, at 1800 hours—storm pattern, representation of the entire Black Sea basin. **a** The *background* shows the significant wave height scalar field and the *foreground* shows wave vectors (*black arrows*) and wind vectors (*white arrows*). **b** The *background* shows normalized wave power and the *foreground* shows energy transport vectors (in kilowatts per metre of wave front). The locations in the computational domain of the maximum values for the significant wave height, wind velocity, and wave power are marked with *circles*

the foreground. Figure 8b shows the normalized wave power in the background and the energy transport vectors in the foreground. For this case study the value of P_{max} was set at 150 kW/m. In this case there is a correspondence between the locations of the maximum significant wave height (6.9 m) and the maximum wave power (142.8 kW/m).

5.3 Case study 3: February 24, 2002, at 0300 hours

This case study, illustrated in Fig. 9, presents average to high energetic conditions for the western medium-resolution computational domain. The geographical extent of this area is shown in Fig. 4 and the boundary conditions are generated using the nesting procedure from model simulations performed for the entire basin of the sea.

Figure 9a presents the significant wave height scalar field in the background and the wave and wind vectors in the foreground. Figure 9b shows the normalized wave power in the background and the energy transport vectors in the foreground. A reference line crossing the most energetic area, which is offshore of the Sulina channel, is also included in the figure. For this case study, the value of P_{max} was set at 50 kW/m. Figure 9c presents the variations along the reference line of some relevant wave parameters (Hs, Cg group velocity, water depth, and wave energy) and, in this way, the energetic peaks can be better observed. The locations of the two maximums ($H_{smax} = 4.9$ m and $E_{TRmax1} = 50.2$ kW/m) are close but do not coincide. A second important observation is that local effects may sometimes induce energetic peaks that exceed the global peak from the coarse area covering the entire Black Sea basin.

5.4 Case study 4: March 11, 2002, at 1800 hours

This last case study, illustrated in Fig. 10, presents the coastal impact of an extreme storm in the western medium-resolution computational domain. Figure 10a presents the significant wave height scalar fields in the background and

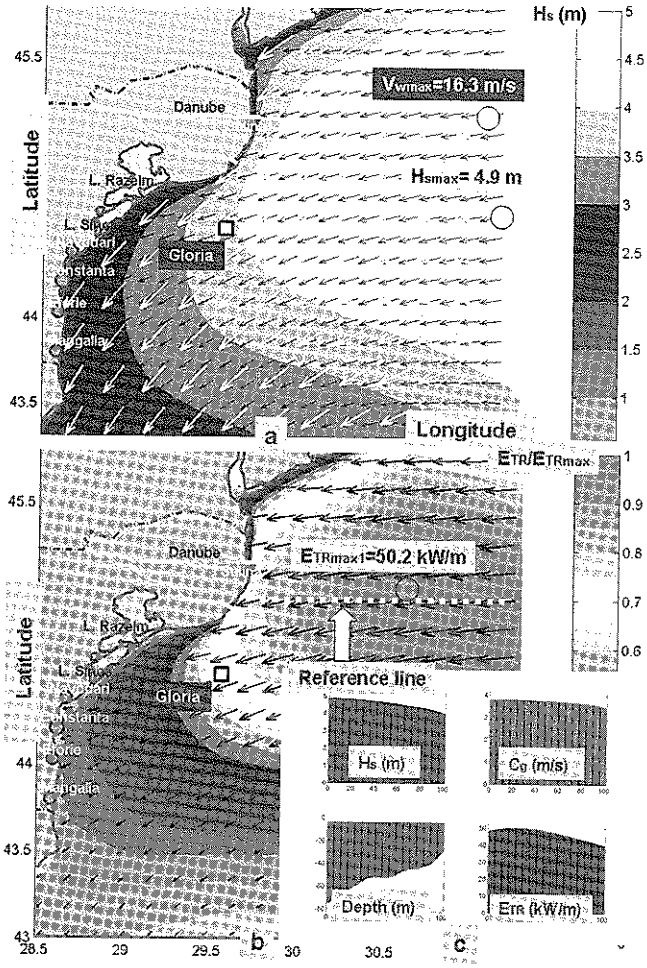

Fig. 9 Case study 3—February 24, 2002, at 0300 hours—average to high energetic pattern, representation for the western coastal computational domain. **a** The *background* shows the significant wave height scalar field and the *foreground* shows wave vectors (*black arrows*) and wind vectors (*white arrows*). **b** The *background* shows normalized wave power and the *foreground* shows energy transport vectors (in kilowatts per metre of wave front); a reference line in the field is also represented. **c** Variation along the reference line of wave parameters [Hs, group velocity (Cg), water depth, and wave energy]. The location in the computational domains of the maximum values for the significant wave height, wind velocity, and wave power are marked with *circles*

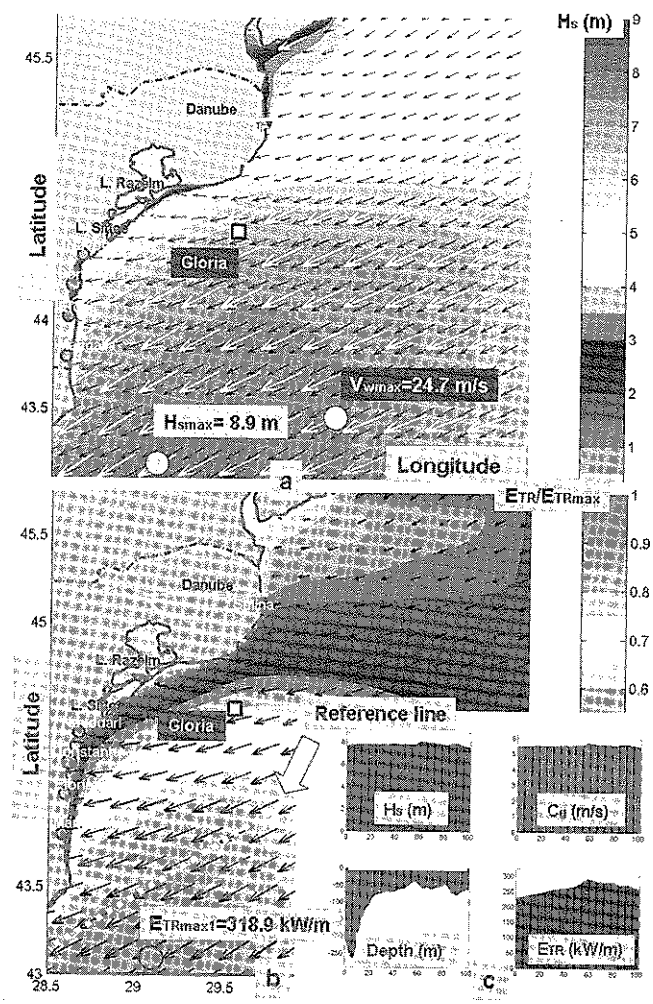

Fig. 10 Case study 4—March 11, 2002, at 1800 hours—extreme wave conditions, representation for the western coastal computational domain. **a** The *background* shows the significant wave height scalar field and the *foreground* shows wave vectors (*black arrows*) and wind vectors (*white arrows*). **b** The *background* shows normalized wave power and the *foreground* shows energy transport vectors (in kilowatts per metre of wave front); a reference line in the field is also represented. **c** Variation along the reference line of wave parameters (Hs, Cg, water depth, and wave energy). The location in the computational domains of the maximum values for the significant wave height, wind velocity, and wave power are marked with *circles*

the wave and wind vectors in the foreground. Figure 10b shows the normalized wave power in the background and the energy transport vectors in the foreground. A reference line crossing the most energetic area, which this time occurs in the southern part of the computational domain, is also included in the figure. For this case study, the value of P_{rmax} was set at 300 kW/m. Figure 10c presents the variations along the reference line of some relevant wave parameters (Hs, Cg, depth, and wave energy). In these variations the energetic peak is evident. The locations of the two maximums ($H_{s\max} = 8.9$ m and $E_{\mathrm{TRmax1}} = 318.9$ kW/m) are very close.

6 Discussion of the results

Some general observations can be made from the analysis of the above case studies. The first observation is that the locations of the energetic peak and the maximum significant wave height do not always coincide. The reason for this is that, while the significant wave height is a function of the energy spectrum only, the wave power depends also on the group velocity, as seen in Eq. 5.

Some near-shore areas characterized by their high energy relative to the rest of the corresponding computational domain also were detected in this analysis. As seen

in Figs. 9 and 10, the richest wave energy resource locations are offshore from the Sulina channel and in the southern part of the medium-resolution computational domain that corresponds to the coastal area from north of the Bulgarian near-shore region.

Rusu and Guedes Soares [19] performed an in-depth analysis of the wave energy spatial distribution in the Portuguese continental near-shore area, which is considered to be among the coastal areas richest in wave energy resources. This analysis was based on in situ measured data for the period 1994–2003 and on simulations with a model system based on WAM for wave generation and SWAN for near-shore transformation in the coastal environment.

Some insight can be gained at this point by comparing the results of that study of the west Iberian coast with those from the present investigation of the Black Sea. First, the maximum values of wave power in the Iberian coastal environment were between 50 and 100 kW/m, while in the Black Sea these values lay between 20 and 50 kW/m. The highest energetic conditions in the Iberian near-shore area were about 600 kW/m, while in the Black Sea they are around 320 kW/m. At the Sines buoy, which is operating in the central part of the Portuguese continental near-shore area, the average value of significant wave height recorded during the period 1994–2003 was about 1.7 m. This is very close to the average value in the Black Sea at the Gloria drilling unit.

In consideration of the above, the Black Sea, which is not generally believed to have substantial wave energy resources, may actually have potential for development—especially on its western side.

7 Final considerations

The potential for wave energy extraction can be determined from analysis of the wave climate. Buoy data can provide a general idea of the existing conditions as well as valuable information concerning some tendencies. Nevertheless, this approach has some limitations, due to the fact that the time period of the measurement is usually limited and the data are obtained in deep water. On the other hand, wave energy can be accurately predicted within a window of a few days using numerical models.

It is of significant interest, therefore, to develop a system that is able to predict wave characteristics in various coastal locations, not necessarily considered as deep water. Toward this end, numerical models not only allow predictions of the wave fields, but also can be forced with atmospheric models and generate long-term hindcasts for periods of about 40–50 years. They can thus provide a means to create a solid statistical base for consistent analysis and wave predictions in both offshore and near-shore zones.

The present work aims to demonstrate the effectiveness of using a wave prediction system based on spectral phase averaging numerical models to assess the spatial distribution patterns of the wave energy in the Black Sea basin. Areas in the coastal environment having good wave energy resources can thus be better identified.

An analysis of the observed wave parameters in the western part of the Black Sea was carried out using data measured in situ. This provided a perspective of the wave climate and the average energetic conditions in the target area. This database of measurements also gives an indication of the extent to which numerical models can be validated in this coastal environment. Following this analysis, a wave prediction system based on spectral phase averaging models was used to evaluate the energetic fields for the entire Black Sea basin, while increasing the spatial resolution shoreward (toward the western coast). Model system simulations were carried out for two time intervals and comparisons against data from two buoys and a wave staff installed at the Gloria drilling platform were performed. Some calibration tests were also accomplished and the most appropriate physics for the Black Sea basin have been identified.

Both direct comparisons and statistical results show the reliability of the wave prediction system that was developed. The wave prediction system has been validated in the present study and can be used with confidence for predictions in various locations of the Black Sea.

References

1. INCDM 1994 Study on the wave and wind climate close the Romanian littoral. Technical report, The Marine Research Institute Grigore Antipa, Constanţa (in Romanian)
2. Coman C (2004) EUROSION Case study technical report http://copranet.projects.eucc-d.de/files/000151_EUROSION_Mamaia.pdf
3. WAMDI Group (1988) The WAM model—a third-generation ocean wave prediction model. J Phys Oceanogr 18:1775–1810
4. Booij N, Ris RC, Holthuijsen LH (1999) A third-generation wave model for coastal regions. Part 1: model description and validation. J Geophys Res 104 C4:7649–7666
5. Stelling GS, Leendertse JJ (1992) Approximation of convective processes by cyclic AOI methods. In: Proceeding 2nd international conference on estuarine and coastal modeling, ASCE Tampa, Florida, pp 771–782
6. Booij N, Holthuijsen LH (1987) Propagation of ocean waves in discrete spectral wave models. J Comput Phys 68:307–326
7. Holthuijsen LH, Herman A, Booij N (2003) Phase-decoupled refraction–diffraction for spectral wave models. Coast Eng 49:291–305
8. Holthuijsen H (2007) Waves in oceanic and coastal waters. Cambridge University Press, Cambridge, p 387
9. Komen GJ, Hasselmann S, Hasselmann K (1984) On the existence of a fully developed wind sea spectrum. J Phys Oceanogr 14:1271–1285

10. Hasselmann K (1974) On the spectral dissipation of ocean waves due to white-cap. Bound-Lay Meteorol 6(1–2):107–127
11. Janssen PAEM (1991) Quasi-linear theory of wind-wave generation applied to wave forecasting. J Phys Oceanogr 21:1631–1642
12. Van Vledder G Ph, Hurdle DP (2002) Performance of formulations for whitecapping in wave prediction models. In: Proceedings of the 21st international conference on offshore mechanics and arctic engineering (OMAE 2002), ASME, Paper OMAE2002-28146
13. Yan L (1987) An improved wind input source term for third-generation ocean wave modelling, Scientific report WR-No 87-8, KNMI, De Bilt, The Netherlands
14. Alves JHGM, Banner ML (2003) Performance of a saturation-based dissipation-rate source term in modelling the fetch-limited evolution of wind waves. J Phys Oceanogr 33:1274–1298
15. Guedes Soares C, Weisse R, Carretero JC, Alvarez E (2002) A 40-year hindcast of wind, sea level and waves in European waters. In: Proceedings of the 21st international conference on offshore mechanics and arctic engineering (OMAE 2002), ASME Paper OMAE2002-SR28604
16. Guedes Soares C (2008) Hindcast of dynamic processes of the ocean and coastal areas of Europe. Coast Eng 55:825–826. doi: 10.1016/j.coastaleng.2008.02.007
17. Valchev N, Pilar P, Cherneva Z, Guedes Soares C (2004) Set-up and validation of a third-generation wave model for the Black Sea, In: Proceedings of 7th International Conference on "BLACK SEA 2004", pp 273–279
18. Hsu SA, Meindl EA, Gilhousen D (1994) Determining the power-law wind-profile exponent under near-neutral stability conditions at sea. J Appl Meteorol 33(6):757–765
19. Rusu E, Guedes Soares C (2008) Wave Energy assessments in the coastal environment of Portugal continental. In: The 27th international conference on offshore mechanics and arctic engineering OMAE 2008, ASME paper OMAE08